Opto-Electronic Science

CN 51-1800/O4   ISSN (Print) 2097-0382   ISSN (Online) 2097-4000

Fiber-optic microstructured sensors based on abrupt field patterns: theory, fabrication, and applications

Yuxuan Yi, Wanlai Zhu, Zao Yi*, Zigang Zhou, Shubo Cheng, Majid Niaz Akhtar and Sohail Ahmad

Citation: Yi YX, Zhu WL, Yi Z, Zhou ZG, Cheng SB, Akhtar MN, Ahmad S. Fiber-optic microstructured sensors based on abrupt field patterns: theory, fabrication, and applications. *Opto-Electron Sci* **5**, 250027(2026).

https://doi.org/10.29026/oes.2026.250027

Received: 30 June 2025;   Accepted: 30 December 2025;   Published online: 23 January 2026

OES | Opto-Electronic Science

Review

January 2026, Vol. 5, No. 1

Open Access

Fiber-optic microstructured sensors based on abrupt field patterns: theory, fabrication, and applications

Yuxuan Yi[1†], Wanlai Zhu[1†], Zao Yi[1,2*], Zigang Zhou[1], Shubo Cheng[3], Majid Niaz Akhtar[4] and Sohail Ahmad[5]

Abstract: Fiber-optic sensing technology has the advantages of passivity, anti-electromagnetic interference, long-distance measurement, high sensitivity and high accuracy, small size, and adaptability to harsh environments such as high-vacuum, high-pressure, and strong magnetic fields compared with the traditional electrical sensing technology. However, with the increasing application requirements, how to further improve the sensitivity of fiber-optic sensors, extend the detection limit and improve the maintenance-free capability has become one of the core issues of the current research. This paper reviews the principle, preparation, and application of fiber-optic microstructured sensing based on abrupt field type. It specifically outlines the development and applications of micro-nano optical fibers, photonic crystal optical fibers, optical fiber gratings and structured optical fibers, and lists the main preparation methods of two types of micro-nano optical fibers from the basic theory of optical fiber microstructured sensor devices.

Keywords: fiber-optic microstructure sensing; sudden field-type fiber-optic microstructure devices; fiber-optic refractive index sensors; micro- and nanofibers; Wiener fiber preparation

DOI: 10.29026/oes.2026.250027 | CSTR: 32246.14.oes.2026.250027

Citation: Yi YX, Zhu WL, Yi Z et al. Fiber-optic microstructured sensors based on abrupt field patterns: theory, fabrication, and applications. *Opto-Electron Sci* **5**, 250027 (2026).

1 Introduction

The wide application of sensor technology in various fields, especially in deep-sea exploration[1], aerospace[2], defence and military industry[3], biomedical[4] and industrial production[5], has become an important part of the development of modern science and technology. With the improvement of industrial automation and intelligence level, the performance requirements of sensors such as accuracy, sensitivity, stability and response speed are getting higher and higher. However, many existing conventional sensing technologies, especially sensors based on electrical, mechanical or chemical principles, still face a number of challenges, especially in terms of adaptability and high-accuracy measurements in complex environments with high temperatures, high pressures, high vacuums, and strong electromagnetic interference. For example, electrical sensors: electrical sensors usually rely on changes in electrical signals, such as resistance and voltage, to detect physical quantities or chemical substances[6]. Although it has a fast response speed, simple structure and low cost, there is strong electromagnetic interference, and its sensitivity and stability are easily damaged in complex environments. In addition, the long-distance transmission signal is easily attenuated, which limits its application in remote monitoring. Mechanical sensors: mechanical sensors such as pressure sensors and displacement sensors usually rely on changes in physical displacement to detect physical quantities[7,8]. Although these sensors have a high resolution, their structure is complex, easy to wear and tear, and they are greatly affected by factors such as ambient temperature and humidity, resulting in poor stability for long-term use. Chemical sensors: chemical sensors use chemical reactions or adsorption phenomena to detect chemical components in gases or liquids[9–11]. Although chemical sensors have important applications in gas

Received: 30 June 2025

Accepted: 30 December 2025

Published online: 23 January 2026

[1]School of Mathematics and Science, Southwest University of Science and Technology, Mianyang 621010, China; [2]School of Chemistry and Chemical Engineering, Jishou University, Jishou 416000, China; [3]School of Physics and Optoelectronic Engineering, Yangtze University, Jingzhou 434023, China; [4]Institute of Physics, The Islamia University of Bahawalpur, Bahawalpur 63100, Pakistan; [5]Institute of Physics, Bahauddin Zakariya University, Multan 66000, Pakistan.

†These authors contributed equally to this work.

*Correspondence: Z Yi, E-mail: yizaomy@swust.edu.cn

detection and environmental monitoring, many traditional chemical sensors have limitations in sensitivity, selectivity, and response time, and are susceptible to interference from environmental factors.

In light of these challenges, fiber-optic sensing technology has gained widespread attention due to its inherent advantages—such as immunity to electromagnetic interference, capacity for long-distance and distributed measurements, compact size, high stability, and superior sensitivity and detection limits[12,13]. These attributes make fiber-optic sensors highly suitable for demanding application environments. In this paper, the multi-application requirements of optical fiber sensing technology are divided into three aspects as shown in Fig. 1. Physical field detection, chemical atmosphere monitoring, and biochemical solution analysis are discussed: when optical fibers are applied to biochemical solution analysis, including blood testing, water contamination screening[14], food safety, and monitoring of biopharmaceuticals, it is necessary to modify a sensitive membrane layer or an antibody, which can specifically bind to the target molecules/ions, onto the optical fiber surface, and then place it in different dispersions to achieve biochemical analysis, as the range of refractive index fluctuations increases due to different types of solutions. The surface of the fiber is modified with a sensitive membrane layer or antibody that can specifically bind the target molecules/ions, and then placed in different dispersions for biochemical analysis[15], which increases the range of refractive index fluctuations that the sensor needs to adapt to due to the different types of solutions. When optical fibers are used for sensing physical fields including temperature, electromagnetic fields, vibration, humidity and stress, it is often necessary to encapsulate the optical fibers with high refractive index materials in order to improve the sensing sensitivity and mechanical properties[16,17], e.g., encapsulation with polydimethylsiloxane or dimethanol improves the temperature sensitivity, and encapsulation with materials such as magneto-fluid improves the sensitivity of magnetic field detection. In applications such as industrial gas leak detection, environmental pollution assessment, air quality evaluation, and cleanroom monitoring, optical fiber sensors are frequently functionalized with gas-responsive materials to enable selective interaction with target molecules[18,19]. Commonly employed coatings include metal-organic frameworks (MOFs), quantum dots, and polymer films. These sensing layers operate in environments where the surrounding refractive index is slightly above unity. The precise monitoring of the target gas composition is then achieved by exposure to an environment with a refractive index of slightly more than 1. In summary, fiber-optic sensing technology holds broad application prospects across multiple domains, particularly in the detection of physical, chemical, and biological parameters.

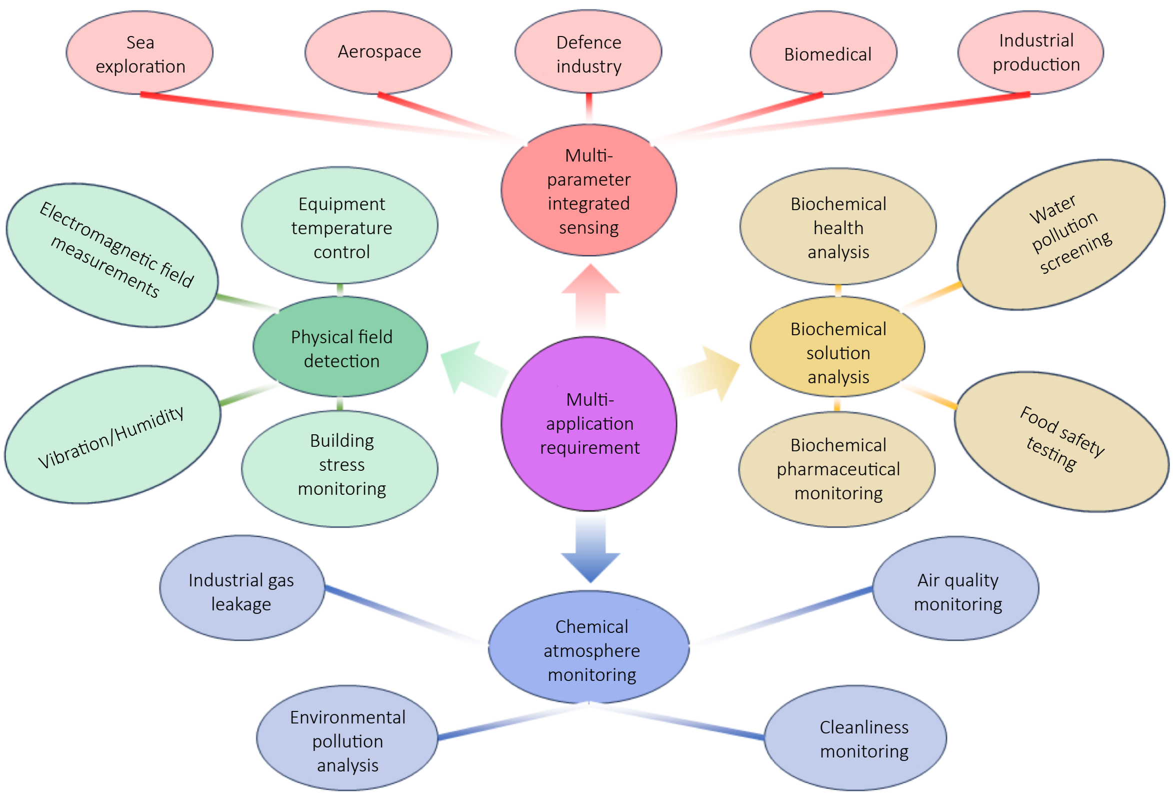

Fig. 1 | Multi-disciplinary sensing application requirements.

By incorporating diverse sensing materials, these sensors offer notable advantages such as high sensitivity, rapid response, and minimally invasive measurement.

In this review, we categorize the applications into three broad groups: (i) physical parameters such as temperature, strain, and refractive index; (ii) chemical and environmental parameters, including gas concentration and solution composition; and (iii) biological and medical applications, such as biomarker detection and biosafety monitoring. This hierarchical classification underpins the organization of the subsequent sections, where each sensing structure is discussed in relation to the corresponding application domain. Among them, fiber-optic microstructured sensors based on the principle of evanescent wave are one of the major research categories and have demonstrated excellent performance in many sensing fields. The core principle of such sensors lies in the interaction between swift waves and the environment, i.e., when a light wave propagates in a waveguide, part of its energy will be rapidly attenuated along the waveguide surface and interacts with the external medium, a characteristic that gives fiber-optic microstructured sensors a significant advantage in detecting weak signals and enhancing sensing sensitivity.

In light of the growing demand for high-performance fiber-optic sensors, this review aims to provide a comprehensive and structured overview of microstructured fiber-optic sensing technologies based on abrupt field interactions. Compared with existing reviews that tend to focus solely on specific device types or applications, this paper highlights three key advantages. It offers a systematic classification of representative device structures, including micron fibers, photonic crystal fibers, fiber gratings, and structured optical fibers, enabling a broad yet detailed understanding of the current landscape. It provides an in-depth discussion of the theoretical basis behind swift wave interaction and absorption mechanisms, which is essential for performance optimization but often underrepresented in general reviews. The review emphasizes mainstream fabrication techniques such as chemical corrosion and high-temperature tapering, bridging the gap between theory and practical implementation. Together, these aspects present a comprehensive and application-oriented perspective that will benefit both new researchers and experienced engineers in the field.

Owing to the pressing demands for sensitivity and environmental resilience in deep-sea exploration and biomolecular detection, transient field fiber optic sensors must overcome the physical limitations inherent in conventional electrical/mechanical sensing. This paper aims to systematically elucidate the synergistic mechanisms governing microstructure design, fabrication processes, and performance optimisation, thereby filling the gap in existing reviews concerning a comprehensive analysis spanning the entire chain from structure to principle to application.

2 Fiber optic micro-structured devices based on abrupt field patterns

As the demand for advanced sensing applications continues to grow, a key focus of current research is on optimizing the performance of fiber-optic sensors—particularly in enhancing sensitivity, response time, detection limits, and signal-to-noise ratio, while also striving to achieve long-term stability and minimal maintenance requirements. These demands have greatly contributed to the development of different configurations of optical fibers, such as photonic crystal fiber (PCF)[20], tilted fiber grating (TFBG)[21], optical resonance cavities (resonance vials[22], resonance rings[23], etc.), fiber optic interferometers (F-P interferometry[24], Mach Zündel interferometry[25], Sagnac interferometry[26]), cascade structures (S-M-S[27], S-SCF-S[28], S-N-S[29], S-H[30], etc.), end-face microstructured types (end-face hypersurfaces[31], end-face cantilever arms[32], F-P cavities[33]), structured optical fibers (D[34], U[35], S[36], J[37], Ω[38]), micro-nano optical fibers[39], etc. The operating principle of the vast majority of fiber optic sensors is based on the Evanescent Wave effect, whereby part of the light energy transmitted by the core of an optical fiber leaks out into the surrounding medium when it comes into contact with the surface of the fiber, and this leaked light field is closely related to the nature of the surrounding environment. Using this phenomenon, optical fibers can be used as highly sensitive sensors to detect the physical, chemical or biological properties of different media. In addition, physical phenomena such as Raman scattering[40], dispersive turning points, echo wall modes[41], surface equipartition excitation resonance[42], and vernier effect[43] have been widely used to enhance the sensing sensitivity.

Fiber optic sensors based on evanescent field type have the advantages of compact structure, high sensitivity, anti-electromagnetic interference, corrosion resistance, etc., and have been widely used in the fields of national defence, new energy, biomedicine, human-computer interaction, etc.[44,45] According to the number of ports of the device, it can be divided into single-ended, double-ended and multi-port; according to the demodulation of signals, it can be divided into intensity demodulation[46,47], phase demodulation[48] and wavelength demodulation type[49–51]. The intensity demodulation type is mainly based on the principle of swift wave absorption, and the environmental variables are resolved by analysing the change of output signal strength. The wavelength demodulation type is mainly based on the swift field excitation of the surface equipartition excitation resonance, and the environmental variables are resolved by analysing the drift change of the resonance peaks; the phase demodulation type is mainly based on the interference formed by the pattern leakage of the strong swift field, and the amount of environmental changes is resolved by analysing the drift of the interference peaks. The key to fiber-optic sensors based on swift field is how to construct structures that can form strong mode leakage in the sensing region, and there are two main ways of leakage, one is to carry out secondary processing of optical fiber modification operations, for example, pulling cone processing, side throwing, etching, bending, corrosion and other operations on optical fiber; the second is to design and prepare special structures such as PCF[52,53], TFBG[54,55] and other new structures[47]. Currently, four typical fiber structures characterized by pronounced abrupt field distributions have been widely studied and developed: micro/nano optical fibers, photonic crystal fibers, tilted fiber gratings, and various structured fiber designs.

2.1 Micro- and nanofibers

Micro- and nanofibers (MNFs) have been extensively investigated, with Prof. Tong and colleagues providing comprehensive demonstrations of their fabrication methods and fundamental optical properties. In this review, we do not aim to repeat those details, but rather to highlight their sensing mechanisms, recent performance improvements, and representative applications within the broader context of abrupt field patterns. This approach allows us to emphasize their role in comparison with other microstructured fibers such as PCFs and gratings. With the deepening of the research on light, especially the enhancement of the requirements on the performance of optical fiber technology and devices, it has become one of the research hotspots in the field of optical fiber to reduce the structure and mode field size of optical fiber, in order to improve its ability of constraining and regulating the light in smaller scale space, and to explore the new mechanism and technology of the interaction between light and matter. As a combination of optical fiber optics and micro-nano technology, micro-nano optical fiber has been developed into a new type of micro-nano waveguide structure in recent years. Compared to conventional optical fibers, micro- and nanofibers have smaller diameters (usually close to or smaller than the vacuum wavelength of transmitted light), larger core-cladding refractive index differences (about 0.5 with the air cladding), and larger swift field strengths, which, despite the presence of a large proportion of the swift field, can still confine the light field in the fiber cross-section to wavelength scales that are close to the optical diffraction limit, as shown in Fig. 2(a). These features endow micro-nano optical fibers with some unique optical transmission properties, such as low loss, high-intensity optical field confinement, strong swift field, surface field enhancement, significant waveguide dispersion, tiny mass and compatibility with standard optical fibers. These advantages provide new possibilities for the application of optical fiber technology in the fields of high-sensitivity optical sensing, microscale high-efficiency near-field coupling, low-power nonlinear effects, low-loss dispersion compensation over short distances, cold-atom manipulation, and ultra-fast optical modulation, as shown in Fig. 2(b).

The guiding modes of micro-nano optical fibers, especially the intensity, phase, and spectral properties of the swift fields transmitted on their surfaces, are very sensitive to small changes in the refractive index of the environment, and are therefore well suited for high-sensitivity optical sensing[58]. Currently, micro-nano fiber optic sensing structures have been widely used to detect a variety of physical, chemical and biological signals, such as concentration, temperature, humidity, deformation, pressure, pH, electric current, etc.[59]. Such sensors offer notable benefits, including enhanced sensitivity, rapid response times, compact form factors, and low power consumption. Considering the

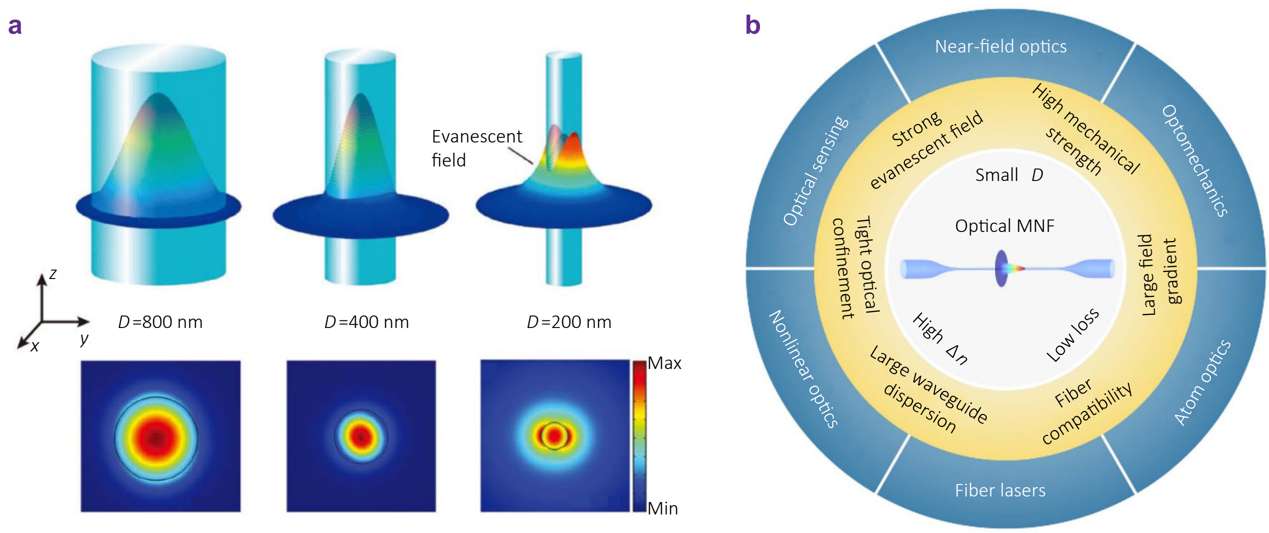

Fig. 2 | (a) Distribution of energy flow (slope-printing vectors) along the axial direction of the transmitted light (top) and the distribution of the cross-section optical field intensity (bottom). (b) Characteristics and potential applications of micro- and nanofibers. Figure reproduced with permission from: ref.[56], American Chemical Society; ref.[57], under a Creative Commons Attribution 4.0 International License.

demand for highly sensitive, tiny and wearable sensors in the fields of robot control, human-computer interaction and healthcare, as well as the challenges of existing 'electronic skin' sensors in terms of electromagnetic interference and response speed, Tong LM's group and Zhang L's group at Zhejiang University have carried out a series of extended applications of micro- and nano-fiber optics[60].

Regarding the more demodulated types of sensors for micro-and nanofibers can be classified into intensity and phase types, several typical micro- and nanofiber configurations are illustrated in Fig. 3. (a) Surface-modified functional film layer type, which is often applied to atmosphere detection or solution analysis, but we need to recognise that the surface modification of the fiber is easily contaminated or destroyed when solution analysis is carried out; (b) excitation of WGM mode type; (c) construction of interferometric mode type, which is the key to constructing phase-type sensing, and is conducive to the improvement of detection sensitivity and detection limit; and (d) single micro-nanofiber strength type, which can be significantly enhanced to improve the mechanical properties and used for mechanical aspects of the measurements; (e) dual nanofiber intensity coupling type, which can significantly improve the mechanical detection sensitivity by changing the coupling efficiency through deformation; (f) multiple nanofiber arrays, which is a composite structure of surface sensing extended by point or line sensing, and can be used for wearable 'electronic skin' sensing.

2.2 Photonic crystal fiber

The development of photonic crystal fibers (PCFs) started in the mid-1990s and is an important innovation in fiber optic technology. The basic concept of PCFs was first proposed by Knight et al. in 1996, who altered the propagation properties of optical fibers by introducing periodically arranged microstructures (e.g., air holes) in the fibers, which in turn gave the photonic crystal fibers a very different optical behaviour. The emergence of PCF breaks the 'total reflection' transmission mode of traditional optical fibers. The introduction of a periodic refractive index variation between the fiber core and cladding allows light transmission to go beyond simple total internal reflection, enabling more accurate manipulation of light propagation via the engineered periodic microstructure. According to the differences in the light guiding mechanism, PCFs can be classified into two categories: total internal reflection PCFs (TIR-PCFs), and photonic bandgap guided PCFs (PBG-PCFs). Its structure is shown in Fig. 4.

The guiding mechanism of TIR-PCF resembles that of traditional optical fibers. By embedding periodically arranged air holes of specific dimensions in the cladding, the effective refractive index of the cladding becomes lower than that of the core, thereby enabling light confinement within the core through total internal reflection. TIR-PCF has a wide wavelength range to maintain a stable normalized transmission frequency, and it is therefore in a wide wavelength range. It is capable of single mode transmission and exhibits different dispersion characteristics. PBG-PCF has a

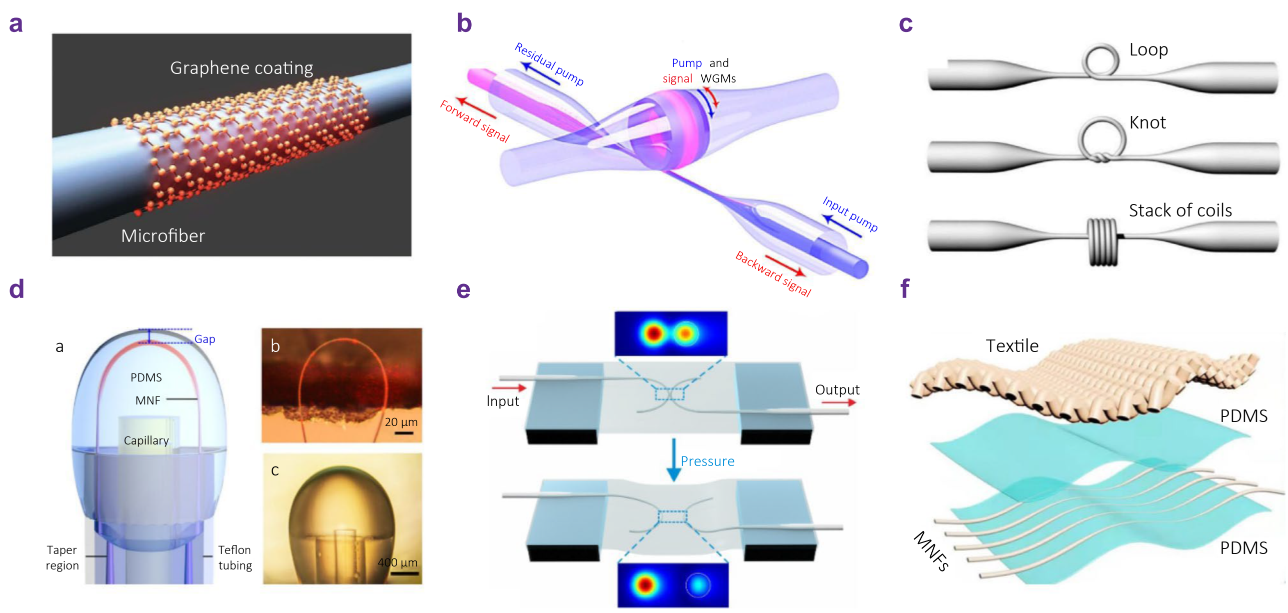

Fig. 3 | Micro-nano-fiber based sensor devices: (a) surface-modified functional film layer type; (b) excitation of WGM mode type; (c) construction of interferometric modes type; (d) single micro-nano-fiber intensity type; (e) dual micro-nano-fiber intensity-coupled type; and (f) multiple micro-nano-fiber arrays type. Figure reproduced from: ref.[61], American Chemical Society; ref.[62], Optical Society of America under the terms of the OSA Open Access Publishing Agreement; ref.[63], American Chemical Society; ref.[64], under a Creative Commons Attribution 4.0 International License; ref.[65], Springer Nature.

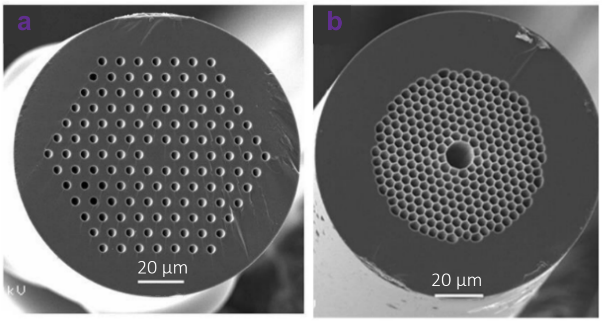

Fig. 4 | (a) Total internal reflection PCF. (b) Band gap guided PCF. Figure reproduced with permissionfrom: ref.[66], Chinese Laser Press.

different design in which the refractive index of the fiber core is lower than the effective refractive index of the cladding. The air holes in the fiber cladding are arranged in a strict periodicity, forming a two-dimensional photonic crystal structure, which in turn creates a photonic bandgap effect. When the frequency of light falls into the bandgap range, light waves cannot propagate through the photonic crystal. The low refractive index fiber core disrupts the overall periodic structure and introduces a narrow band of defect states inside the PCF. This defect state allows light in a specific frequency range to be bound within the fiber core, thus enabling its propagation through the core.

However, when the air holes of the TIR-PCF are filled with a material with a higher refractive index than silica, the cladding contains both dielectric columns with higher refractive indices and periodically arranged low refractive index regions, forming a structure with both total internal reflection and photonic bandgap light-conducting mechanisms, which makes the PCF able to propagate light-conducting by using total internal reflection and photonic bandgap effects at the same time[67,68]. By combining the advantages of the two light-guiding mechanisms, PCFs can be applied in various fields, including dispersion compensation, wavelength division multiplexing and demultiplexing, and optical fiber sensing.

With the in-depth study of PCF, it shows unprecedented flexibility and superiority in optical transmission, especially PCF can achieve a high degree of adjustment of light wavelengths, modes, and interactions between light and the environment, which has led to a wide range of research and applications in many fields, such as optical communications, optical sensing, and laser design. PCF offer significantly greater structural design flexibility compared to conventional optical fibers, which makes them particularly well-suited for the development of high-sensitivity optical sensors. Figure 5 shows the more common design approaches for PCF: (a) for TIR-PCF utilizing surface modification and ionic liquid infiltration, ensuring uniform coating on the inner walls of the air holes presents a significant challenge due to their extremely small dimensions; (b) PBG-PCF based on the modification of fluorescent thin film, where the gas to be detected is in direct contact with the sensitive film layer, which can significantly improve the sensing sensitivity, but there is also a problem of uniformity of modification; (c) single-core PCF based on SPR effect, constructing a mismatch structure that always has limited interaction with the environment although it transfers part of the fiber core energy to the cladding layer; (d) multi-core PCF based on SPR effect, which also suffers from low detection sensitivity; (e) although the dual-core photonic crystal

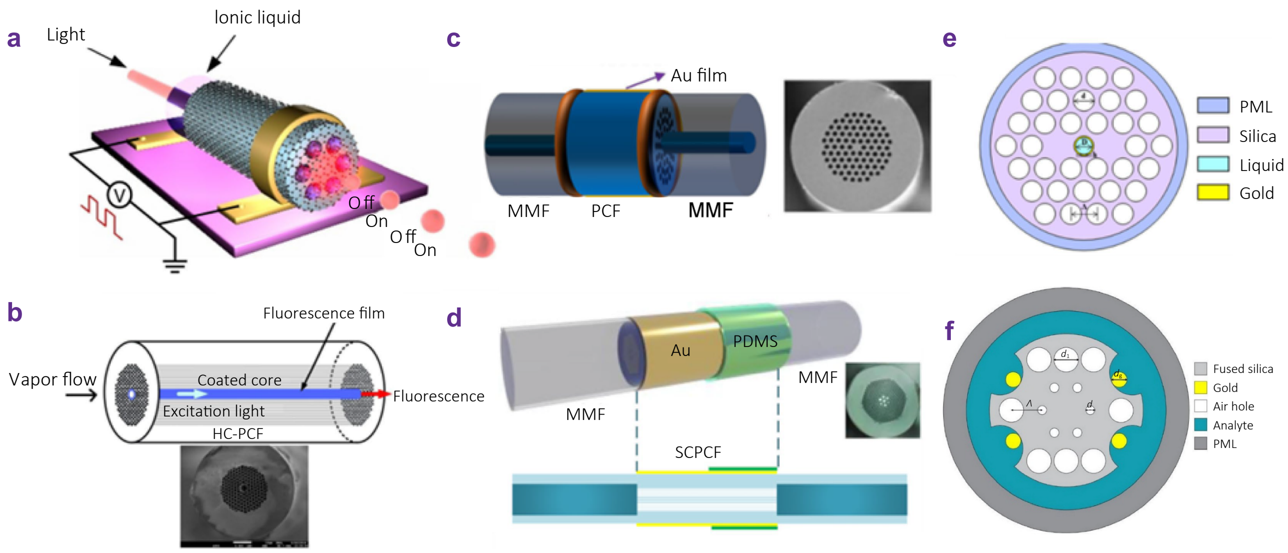

Fig. 5 | (a) TIR-PCF based on surface modification and ionic liquid filling. (b) PBG-PCF based on fluorescent film modification. (c) Single-core PCF based on SPR effect; (d) multi-core PCF based on SPR effect. (e) Dual-core PCF based on air in-pore modification and filling. (f) Functionally oriented design based on SPR-PCF. Figure reproduced from: ref.[69], Springer Nature; ref.[70], Elsevier B.V.; ref.[71], Elsevier B.V.; ref.[72], Elsevier B.V.; ref.[73,74], Optica Publishing Group under the terms of the Optica Open Access Publishing Agreement.

fiber (PCF) based on inner air-hole modification and liquid infiltration can significantly enhance sensing sensitivity, it presents major limitations in practice. Specifically, precise control over the deposition of the gold film is nearly unachievable within the confined structure, and the sensing process requires the target liquid to be accurately filled into specific micro-holes, which further reduces the practical feasibility of this approach; (f) SPR-PCFs based on functionally oriented design, a structure that allows PCFs not to have strict photonic crystal properties and greatly improves the degree of design freedom. The free design of air holes, the free polishing design of the fiber morphology, and the customization of the surface modification can effectively reduce the process difficulty and promote the feasibility of the process while maintaining the high sensing sensitivity.

2.3 Fiber grating

Fiber grating is a new type of grating inscribed inside the optical fiber, can be achieved without changing the structure of the optical fiber itself under the premise of the signal light energy from the optical fiber core to the optical fiber cladding effectively coupled to achieve high mechanical properties, high efficiency and high stability of the optical fiber sensing. The grating structures inscribed in the center core of an optical fiber can be divided into the following types: fiber Bragg grating (FBG), tilted fiber Bragg grating (TFBG) and long period fiber grating (LPFG).

Figure 6 illustrates the representative structures and spectral responses of FBG, TFBG, and LPFG, where the FBG exhibits narrowband Bragg reflection with a corresponding transmission dip due to core–core mode coupling, the TFBG shows densely distributed multi-order resonances arising from strong core-to-cladding mode coupling, and the LPFG presents a few broad attenuation bands in the transmission spectrum resulting from co-propagating core–cladding mode coupling. FBG confine the optical signal within the fiber core by coupling the forward- and backward-propagating core modes, thereby limiting light from reaching the cladding and hindering direct interaction with the external environment. Therefore, to enhance its swift field, it needs to be side-polished or hydrofluoric acid etched to enhance the swift field and its interaction with the environment[75]. TFBG not only provides the Bragg reflection mode of the core, but also enables the core mode to be strongly coupled with a large number of cladding modes, showing an optical comb-like transmission spectrum. Each resonance peak corresponds to a specific cladding mode, which is highly responsive to changes in the refractive index of the medium surrounding the fiber surface. Monitoring shifts in these resonance peaks enables sensitive detection of external environmental variations[76]. However, the resonance peaks are spaced only a few nanometers apart and lack a fixed reference point, limiting their effectiveness over a wide refractive index range. However, the spacing between the resonance peaks is only a few nanometres and there is no reference point, which is not conducive to measurements over a large refractive index range. The LPFG has a large refractive index modulation period that couples the forward-transmitting core mode to the forward-transmitting cladding mode, and its transmission spectrum exhibits a small number of broader resonance peaks of the FWHM in the range of hundreds of nanometres. Due to structural limitations, it not only exhibits high sensitivity to ambient refractive index, but also is susceptible to ambient temperature or bending stress[77].

Combining the highly sensitive SPR effect sensing technique with fiber-optic grating with strong cladding film coupling characteristics provides a new method for ultra-high sensitivity in-situ analysis. Since TFBG and LPFG have

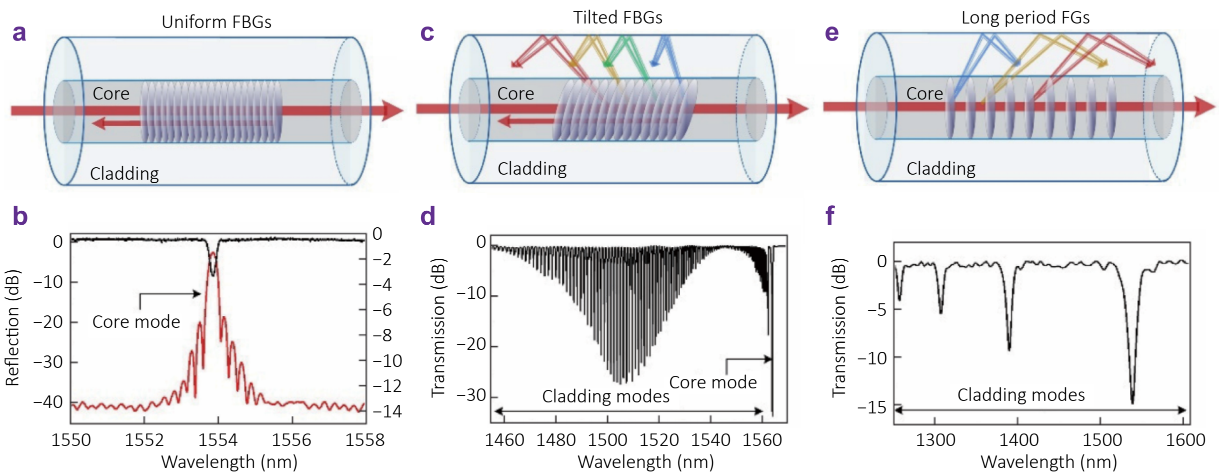

Fig. 6 | (a, b) Bragg grating structures and their transmission (black) and reflection (red) spectra. (c, d) Tilted fiber grating structures and their reflection spectra. (e, f) Long-period fiber grating structures and their transmission spectra. Figure reproduced with permissionfrom: ref.[78], under a Creative Commons Attribution 2.0 International License.

stronger cladding mode coupling ability, they have been expanded for more applications[79]. As shown in Fig. 7(a) and 7(b), the introduction of SPR effect in TFBG can provide a reference point for the extremely dense optical comb spectra while enhancing the sensitivity, based on which, Guo T's group at Jinan University has carried out a series of fiber-optic grating applications for the monitoring of thermal runaway management of batteries. The resonance peaks of LPFGs have a large FSR, which is an advantage in sensing, as shown in Fig. 7(c) shows, the modification of antibody on its surface can effectively improve the detection sensitivity of the sensor to the receptor molecules. Figure 7(d) then demonstrates the fabrication of LPFGs using a micro-nano optical fiber with graphene oxide modified on the surface to improve the desorption capacity and ZIF-90 to improve the specific adsorption capacity, ultimately achieving an acetone sensing sensitivity of 26.1 pm/ppm, which is complicated to prepare and needs to be improved in terms of its universality.

In addition to conventional FBGs, LPFGs, and TFBGs, several emerging grating structures have been developed to extend the sensing capabilities of fiber gratings. One representative example is the excessively tilted fiber Bragg grating (Ex-TFBG), in which the grating planes are inscribed at a large tilt angle (typically >70°). Ex-TFBGs enable strong coupling to high-order cladding modes, producing a broad and highly sensitive spectral response that is particularly advantageous for biochemical sensing and refractive index monitoring.

Another important category is localized fiber gratings, which are fabricated with highly confined modulation regions, often using femtosecond laser inscription. These localized gratings offer flexible inscription geometries and can be integrated at specific points of a fiber device, providing high spatial resolution and adaptability in harsh environments.

The inclusion of these advanced grating types complements the classification framework and highlights the diversity of fiber grating designs, each optimized for distinct sensing requirements. Their applications further enrich the scope of fiber-grating-based sensing, ranging from label-free biosensing to high-temperature and high-strain monitoring.

2.4 Structured optical fibers

The photonic crystal fibers and fiber gratings described in the previous section require specialised equipment, so a series of secondary structural designs for ordinary fiber structures have been derived to enhance the swift field and thus the sensing sensitivity, as shown in Fig. 8(a) shows a multimode interference structure based on a single-mode-coreless-single-mode composition after macrobending, where the angle of the incident light can be changed by macrobending to produce a stronger and more abrupt passing field, and modification by ZnOHF-ZnO to further enhance the environmental interaction capability, and finally a detection limit of 1 ppm for triethylamine was achieved, but the spectral irregularities of this structure are very large and the FSR is very large. Figure 8(b) and 8(c) demonstrates a temperature sensor made by transversely polishing the central part of a multimode optical fiber to form a side-polished optical fiber with a leakage window and by modifying hyperbolic metamaterials, nano-diamonds,

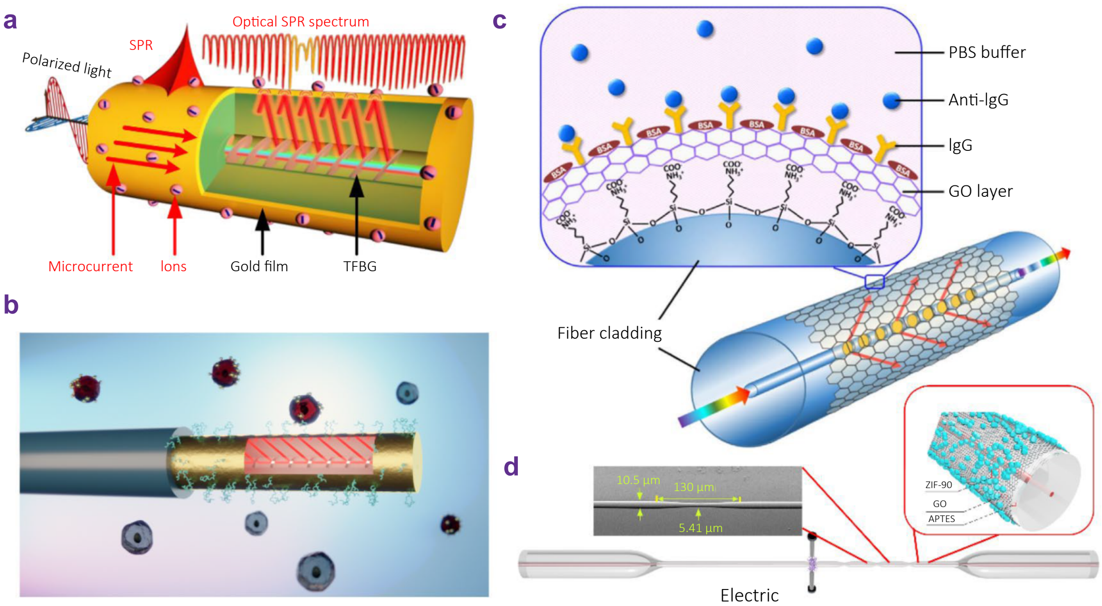

Fig. 7 | (a) SPR-type TFBGs for battery monitoring. (b) SPR-type TFBGs for bioanalysis. (c) Surface antibody-modified LPFGs for biosensing. (d) Surface-modified micro-nano LPFGs for organics gas sensing. Figure reproduced from: ref.[76], under a Creative Commons Attribution 4.0 International License; ref.[80], American Chemical Society; ref.[81], Elsevier B.V.; ref.[82], Elsevier B.V..

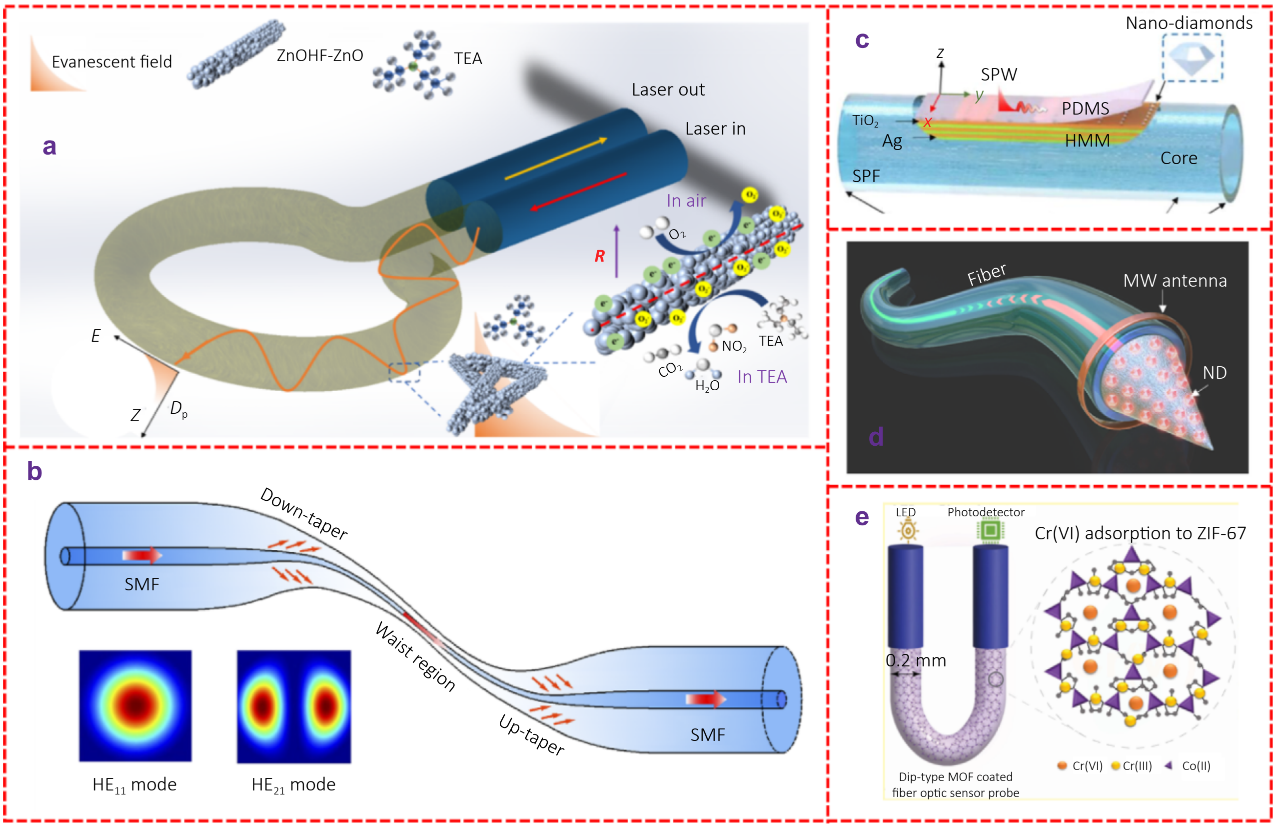

Fig. 8 | (a) Multimode interferometric structure based on single-mode-coreless-single-mode structural composition after macrobending. (b) Z-type based on micro-nano fiber. (c) D-type based on multimode-coreless-multimode side-throwing. (d) Spike-conical type based on multimode optical fiber. (e) U-bending type based on multimode optical fiber. Figure reproduced from: ref.[83], Elsevier B.V.; ref.[84], Optical Society of America under the terms of the OSA Open Access Publishing Agreement; ref.[85], American Chemical Society; ref.[86,87] American Chemical Society.

and PDMS, with a maximum sensitivity of 9.021 nm/°C. However, this sensor preparation process is multi-processed and requires a high degree of process precision, which is not conducive to large-scale reproduction. Figure 8(d) demonstrates a sensor in which a multimode optical fiber was chemically etched to form a tapered tip to enhance the ability of light to interact with the ambient medium and modified with a series of pre-treatment modifications to modify the magnetic field and magnetic substance on nanodiamonds, achieving a sensitivity of 0.57 nT/Hz1/2@1 Hz. Figure 8(e) illustrates a U-shaped macrobending of a decoated multimode optical fiber, which enhances evanescent field intensity by altering the incident angle of light within the bent section. Additionally, an in-situ growth of the porous metal-organic framework material ZIF-67 is performed in this U-shaped region, enabling detection of Cr(VI) ions down to a 1 ppb limit.

2.5 Advantages and limitations of typical fiber microstructures

Different fiber microstructures exhibit distinct advantages and limitations in evanescent-field-based sensing, which largely determine their suitability for specific sensing scenarios. A clear understanding of these trade-offs is essential for rational sensor design and practical deployment.

Micro-/nano-fibers offer extremely strong evanescent-field interaction and fast response due to their subwavelength-scale diameters, making them highly attractive for ultra-high-sensitivity biochemical and refractive-index sensing. Their large surface-to-volume ratio also facilitates efficient surface functionalization. However, micro-/nano-fibers are mechanically fragile and susceptible to environmental perturbations, surface contamination, and long-term signal drift. As a result, robust packaging, surface passivation, and reference-based interrogation schemes are often required to improve their stability in practical applications.

Photonic crystal fibers (PCFs) provide unique structural advantages arising from their periodic air-hole cladding or hollow-core designs. The presence of microchannels enables extended light-matter interaction lengths and efficient gas infiltration, making PCFs particularly well suited for gas and vapor sensing. In addition, their modal properties can be engineered to enhance sensitivity or enable multi-parameter sensing. Nevertheless, PCF-based sensors face challenges related to uniform inner-hole coating, repeatable filling processes, and reliable sealing and interconnection, which currently limit large-scale fabrication and field deployment.

Fiber grating-based structures, including fiber Bragg gratings (FBGs), long-period fiber gratings (LPFGs), and tilted fiber Bragg gratings (TFBGs), are widely used due to their well-defined spectral features and mature fabrication technology. FBGs are especially advantageous for physical-quantity sensing, such as temperature, strain, and pressure, owing to their mechanical robustness, excellent repeatability, and multiplexing capability. LPFGs and TFBGs, which involve strong cladding-mode coupling, are more suitable for refractive-index and biochemical sensing, particularly when combined with surface plasmon resonance or functional coatings. However, grating-based sensors may suffer from cross-sensitivity, polarization dependence, and spectral complexity, necessitating careful structural design and advanced demodulation strategies.

Overall, no single fiber structure is universally optimal for all sensing tasks. Instead, the selection of a specific fiber microstructure should be guided by a balanced consideration of sensitivity requirements, environmental robustness, fabrication feasibility, and the targeted sensing application.

To further illustrate how the structural characteristics and sensing mechanisms discussed above translate into practical sensing performance, a quantitative comparison of representative fiber-optic microstructured sensors is summarized in Table 1[88–96]. The table provides an overview of typical performance metrics, including sensitivity enhancement strategies, detection limits, response times, and application scenarios, for different fiber architectures. By presenting these parameters in a unified format, Table 1 highlights the trade-offs among sensitivity, dynamic response, and robustness across various sensing structures, and offers readers a practical reference for selecting suitable fiber-optic sensor configurations for specific sensing tasks.

3 Theory of fiber-optic sensing based on swift waves

To facilitate a clear correspondence between the fiber structures introduced in Section 2 and the sensing principles discussed in this section, the sensing mechanisms are analyzed here from a structure-oriented perspective. In evanescent-field-based fiber sensors, the dominant sensing response is jointly determined by the optical field distribution, the modal coupling pathway, and the interrogation observable (e.g., intensity, wavelength, phase, or linewidth). These factors are inherently linked to the underlying fiber microstructure.

Different fiber architectures naturally favor different sensing mechanisms. For example, optical micro-/nano-fibers primarily rely on strong evanescent-field interaction and are therefore well suited for absorption-based sensing, surface binding detection, and resonance-enhanced schemes. Photonic crystal fibers enable extended light-matter interaction through their microstructured air-hole regions, making them particularly advantageous for gas and chemical sensing based on absorption, refractive-index variation, or surface plasmon resonance. Fiber gratings, including FBGs, LPFGs, and TFBGs, provide well-defined spectral features and mode-coupling characteristics, which are commonly exploited for wavelength-based interrogation, multi-parameter sensing, and differential measurement schemes.

Based on these considerations, the sensing mechanisms discussed in this section are not treated as isolated physical effects. Instead, each mechanism is analyzed in conjunction

Table 1 | Performance comparison of representative fiber-optic microstructured sensors.

Sensor type	Sensitivity enhancement technology	Typical detection limit	Response time	Application scenarios
Micro-/nanofibers (MNF)[90,96]	Diameter tapering, surface functionalization (Au, graphene, nanoparticles), WGM resonance	10^{-9}–10^{-6} RIU; biomolecule LOD in fM–pM range	<1 s (optical), often limited by analyte diffusion	Biochemical solutions, wearable devices, biosensing
SPR-coated MNF[89,93]	Metal film/nanostructure deposition for SPR excitation	10^{-6}–10^{-9} RIU; biomolecule LOD pM level	Seconds–minutes	High-sensitivity biochemical sensing
Hollow-core/suspended-core PCF[91,92]	Gas/liquid filling into microchannels, photonic bandgap design	ppb-level for gases (e.g., ~2 ppb acetylene); 10^{-6}–10^{-4} RIU for liquids	1–10 s (gas diffusion limited)	Gas sensing, trace spectroscopy
SPR-PCF[92]	Metal thin-film coating or nanostructure inside PCF	10^{-9}–10^{-7} RIU; biomolecule LOD pg·mL^{-1}–ng·mL^{-1}	Seconds–minutes	Chemical/biological liquid detection
Tilted Fiber Bragg Grating (TFBG)[88,95]	Strong cladding mode coupling, SPR or thin-film integration	10^{-6}–10^{-3} RIU; temperature/strain ~0.01–0.1 nm/°C	10 ms–s	Temperature, strain, biochemical monitoring
Fiber Bragg Grating (FBG)[88]	Side-polishing/etching, composite encapsulation	Temp. res. ~0.001–0.1 °C; strain in με range	ms (instantaneous)	Structural health monitoring, long-term temp./strain sensing
Side-polished/D-shaped fibers[89,93]	Side-polishing + SPR/functional films	10^{-7}–10^{-5} RIU; several 10^3 nm/RIU reported	<1 s	Surface biochemical sensing, online liquid monitoring
U-/S-/J-/Ω-shaped bent fibers[94,91]	Macro-bending, angle tuning, functional coatings	ppb–ppm for gases/ions; 10^{-6}–10^{-4} RIU for liquids	<1 s–seconds	Wearable, field gas monitoring, low-cost sensors

with the fiber structures that most effectively support it. A mapping between representative fiber microstructures, their dominant sensing mechanisms, and typical interrogation observables is summarized to provide readers with an intuitive framework for understanding how structural design choices translate into sensing performance. This structure-mechanism-response relationship also serves as a practical guideline for selecting and designing fiber-optic sensors for specific sensing scenarios.

The sensing mechanism relying on evanescent wave absorption is governed by the leakage or loss of electromagnetic energy at the interface between the core and cladding during total internal reflection (TIR). This section focuses on the relevant physical fields and the key parameters that influence the operation of these sensors.

3.1 Sudden wave theory

The optical signal propagates within the waveguide or fiber via total internal reflection, with its transmission influenced by the refractive indices of the core and cladding. This behavior can be described using the critical angle (θ_c) and numerical aperture (NA) as follows[97].

$$\theta_c = \arcsin\left(\frac{n_{clad}}{n_{core}}\right) , \tag{1}$$

$$NA = \sqrt{n_{core}^2 - n_{clad}^2} . \tag{2}$$

The number of supported modes (M) depends on the NA, the fiber radius (r) and the wavelength of the optical signal (λ), and this relationship is given by the following equation[98].

$$M = \frac{4V^2}{\pi^2} \approx \frac{V^2}{2.5} , \tag{3}$$

where $V = 2\pi rNA/\lambda$ is known as the V-number of the fiber and helps to determine the operation of the fiber, i.e. single mode or multi-mode.

Multiple physical, optical, and geometrical characteristics of optical fibers influence the evanescent wave. Among these, the penetration depth and the evanescent power (or the fraction of power residing in the cladding) are key parameters for assessing the performance of EWA sensors.

The depth of penetration (d_p) of a swift wave, the distance by which the electric field amplitude decreases to 1/e of its value at the interface, increases as the refractive index contrast at the core-cladding interface decreases, which is also a function of the wavelength of the light and the angle of incidence[99−101]:

$$d_p = \frac{\lambda}{2\pi n_{core}^2\sqrt{\sin^2\theta_i - \sin^2\theta_c}} = \frac{\lambda}{2\pi\sqrt{n_{core}^2\sin^2\theta_i - n_{clad}^2}} . \tag{4}$$

In theory, evanescent waves can interact with molecules at infinite distances, albeit with diminishing intensity. Practically, the d_p defines the effective range within which molecules significantly influence the sensing signal.

Sudden power (fractional power in the cladding) can be approximated by calculating the fractional power present in the cladding of a multimode fiber[102]:

$$\frac{P_{clad}}{P} = \frac{4}{3\sqrt{M}} = \frac{4\sqrt{2}}{3V} , \tag{5}$$

where P_{clad} is the optical power in the cladding and P total optical power in the core and cladding. From Eq. (5), it can be seen that an increase in the value of V decreases the fractional power in the cladding[103]. Therefore, the choice of V number is very important to determine the swift wave power of the fiber optic sensor.

3.2 Fiber optic sensing principle based on swift wave excitation of surface equipartition exciton resonance

Surface Plasmon Polariton (SPP) is a collective oscillation of electrons at the metal-dielectric interface with a specific longitudinal wave vector $\boldsymbol{k}_{sp}$, which is related to frequency as follows[104,105]:

$$\boldsymbol{k}_{sp}(\omega) = \frac{\omega}{c}\sqrt{\frac{\varepsilon_m(\omega)\varepsilon_d(\omega)}{\varepsilon_m(\omega)+\varepsilon_d(\omega)}} , \tag{6}$$

where $\varepsilon_m = \varepsilon'_m + i\varepsilon''_m$, $\varepsilon_d = \varepsilon'_d + i\varepsilon''_d$, denote the complex dielectric function of metals and dielectric materials, ω is the angular frequency, c is the speed of light in vacuum, the equation is also known as the dispersion equation of SPP.

3.3 Fiber optic sensing principle based on swift wave absorption

The penetration depth of the evanescent wave is very limited, primarily influencing the weak cladding modes while leaving the core modes largely unaffected. To enhance sensing sensitivity, it is essential to optimize the sensing region so that the evanescent field associated with the core mode can directly interact with the analyte[106,107]. When designing fiber-optic sensors based on evanescent wave absorption, understanding the different types of signal loss occurring during transmission is crucial:

1) Refractive loss

In a de-cladded fiber optic probe, an increase in refractive index near the sensing (de-cladded) region reduces the local numerical aperture, resulting in light attenuation caused by refractive losses. Figure 9 illustrates the refractive loss in a fiber optic sensor, where the de-cladding fiber directs some rays (R_1 and R_2) according to the critical angle when it remains in the RI medium (n_2). When the surrounding refractive index changes from n_2 to n_3 (n_3>n_2), the critical angle increases accordingly. As a result, the new critical angle (θ'_c) exceeds the incident angle of ray R_1, leading to its refraction out of the fiber and subsequent loss, as illustrated in Fig. 9(b). Based on the Fresnel reflection coefficient, a portion of the incident light is reflected back into the fiber at each interaction with the core surface, continuing to propagate with diminished power.

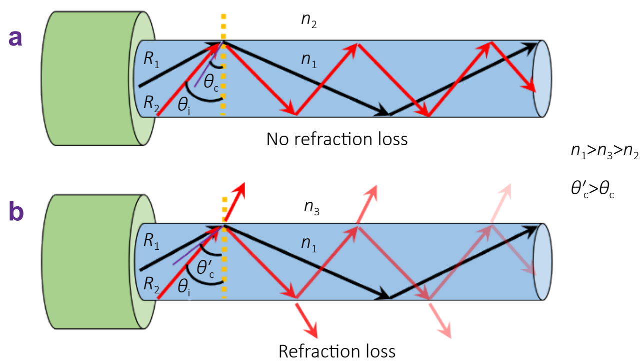

Fig. 9 | Schematic representation of the refractive loss of the fiber optic sensor due to the change in the surrounding RI. (a) No refractive loss occurs due to the $\theta_i > \theta_c$ of the two rays. (b) The RI changes from n_2 to n_3 (n_3>n_2) which increases the critical angle to (θ'_c) and results in the refractive loss of ray R_1. The decrease in the colour intensity of ray R_1 indicates a decrease in the power of the refracted rays. Figure reproduced with permissionfrom: ref.[108], Springer Nature.

Refraction loss arises from an increase in the effective refractive index within the sensing region. For the sensor, this loss can be quantified using the following equation[109,110]:

$$P_{\mathrm{RL}} = -10\log\left(\frac{NA_{\mathrm{a}}}{NA_{\mathrm{r}}}\right)^2 , \tag{7}$$

where P_{RL} is the refraction loss (dB), NA_{a} is the numerical aperture of the sensing region in the presence of the analyte, and NA_{r} is the numerical aperture of the sensing region in the presence of the reference medium. This refractive loss is the synchronous response of the fiber due to changes in the overall RI.

2) V-number mismatch

When light transfers between two optical fibers with different V-numbers (caused by variations in core radius or core/cladding materials, as illustrated in Fig. 10) signal loss can occur. This is because the receiving fiber, having a lower V-number, cannot support the higher-order modes present in the transmitting fiber, leading to loss of the energy carried by those modes.

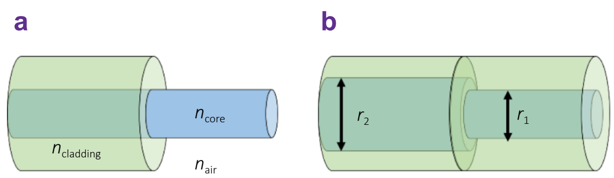

Fig. 10 | Schematic diagram of V-number mismatch. (a) Due to different cladding materials (NA mismatch). (b) Due to different core radii (r_1<r_2).

As shown in Fig. 10(a), when light propagates from a high numerical aperture fiber (NA_1) to a fiber with a low numerical aperture (NA_2), it results in a loss of light. The loss due to mismatch (P_{L}) can be calculated by the following equation[111]:

$$P_{\mathrm{L}} = -10\log\left(\frac{NA_2}{NA_1}\right)^2 . \tag{8}$$

In swift wave absorption-based sensors, the de-cladded sensing region is typically followed by a standard cladding fiber, resulting in a V-number mismatch between the two sections. When light transitions from the sensing region back into the passive fiber, higher-order modes that cannot be coupled are lost, leading to signal attenuation and a reduced signal-to-noise ratio. A common strategy to mitigate this issue is to reduce the core radius of the output fiber to match the V-number. The condition for minimizing V-number mismatch can be expressed by the following equation[112]:

$$r_{\mathrm{a}} \le r_{\mathrm{clad}}\left(\frac{n_{\mathrm{core}}^2 - n_{\mathrm{clad}}^2}{n_{\mathrm{core}}^2 - n_{\mathrm{analyte}}^2}\right)^{\frac{1}{2}} , \tag{9}$$

where r_{a} is the radius of the fiber core at the end of the sensing region, r_{clad} is the radius of the cladding, n_{clad} is the RI of the fiber core, n_{clad} is the RI of the cladding, and n_{analyte} is the effective RI due to the presence of the analyte in the sensing region. Thus, the sensor response of the fiber optic sensor based on swift wave absorption is the combined effect of the loss of refractive index, the mismatch of the V-number swift, and the loss due to the swift wave absorption.

3) Sudden wave absorption loss

In a de-cladded fiber, the evanescent wave at the core surface can interact with the surrounding medium, though its reach is confined by a limited penetration depth. If absorbing molecules are present within this interaction region, they will attenuate the evanescent field, leading to a reduction in the amplitude of the guided mode in the core. The transmitted power at the output end of the de-cladded fiber can be described by the following equation[113]:

$$P_L = P_0 \times \mathrm{e}^{-\gamma L} , \tag{10}$$

where L is the length of the de-cladding fiber probe, P_L is the output optical power after passing through the transmission length (L), P_0 is the initial optical power before passing through the fiber transmission, and γ is the swift wave absorption coefficient of the molecule. The evanescent wave absorption coefficient is directly proportional to the fraction of optical power present in the cladding (or surrounding medium in a de-cladded fiber), the molecular concentration C, and the intrinsic absorption coefficient α. This relationship can be described by the following expression[114]:

$$\gamma = \frac{P_{\mathrm{clad}}}{P}\alpha C . \tag{11}$$

4 Main preparation methods of micro-nano optical fiber

4.1 Chemical corrosion method

The main component of optical fiber is SiO_2, which is chemically very stable, and only hydrofluoric acid can react with it to achieve the purpose of etching in common laboratory drugs. It is difficult to control the etching rate, and the surface of the optical fiber is rough, which leads to large optical loss, so a low concentration of hydrofluoric acid or ammonium fluoride is generally used as a hydrofluoric acid buffer in the experiments to reduce the etching rate of hydrofluoric acid on SiO_2[115]. A common hydrofluoric acid etching optical fiber device is shown in Fig. 11[116]:

$$SiO_2 + 4HF = SiF_4 + 2H_2O \ ,$$
$$SiO_2 + 6HF = H_2SiF_6 + 2H_2O \ . \tag{12}$$

A standard optical fiber with the coating layer removed is fixed on top of the etching platform and an appropriate concentration and volume of hydrofluoric acid solution is added dropwise at its center. Due to surface tension, hydrofluoric acid forms droplets and flows along the surface of the optical fiber during the etching process. By adjusting the distance of the optical fiber within the droplet, the etching length of the micro-nano optical fiber can be precisely controlled. The whole experiment lasts for about 75 minutes, and the hydrofluoric acid needs to be carefully recovered after completion. The hydrofluoric acid etching method is simple and inexpensive to operate, and the droplets are able to move axially on the surface of the fiber, prompting the fiber to naturally form a tapered structure, so many studies have focused on this method in recent years. At present, nanoscale micro-nano optical fibers with high sensitivity and low loss have been successfully prepared. However, this method still faces some challenges, such as the inhomogeneity of the fiber diameter, the difficulty in preparing long-distance micro- and nanofibers, the higher surface roughness compared with the heating method, and the large differences in experimental process parameters, which make it difficult to unify the standards. These issues limit the commercial application of the hydrofluoric acid etching method, which is currently mainly suitable for small-scale preparation in the laboratory.

Although hydrofluoric acid etching is simple to operate and low in cost, it presents significant limitations in practical application:

Surface roughness and optical loss: following etching with low-concentration hydrofluoric acid (5%–10%), the surface roughness R_a of optical fibres typically exceeds 5 nm (compared to R_a<1 nm achieved by the high-temperature taper method). This results in increased optical transmission loss of 3–5 dB/m. Particularly for micro-nanofibres (diameter < 500 nm), the loss is further amplified, limiting their application in long-distance sensing.

Poor diameter uniformity: influenced by surface tension, hydrofluoric acid droplets flow unevenly along the fibre axis, resulting in post-etching diameter deviations of ±50 nm. Sensitivity variations exceeding 15% occur within batches, rendering it difficult to meet mass production consistency requirements.

Challenges in producing extended lengths: limited droplet coverage (typically < 1 cm) precludes fabrication of micro/nanofibres exceeding 2 cm in length. Environmental monitoring applications (e.g., gas concentration distribution) often require sensing areas exceeding 5 cm, thereby restricting practical deployment scenarios.

Safety and process controllability: hydrofluoric acid is highly corrosive, necessitating stringent protective measures during experiments. Etching rates are significantly influenced by temperature (increasing by 10% per 1 °C rise) and humidity, making it difficult to standardise process parameters across laboratories and lacking a standardised fabrication workflow.

4.2 High-temperature molten cone drawing method

The fusion taper method is to remove the coating layer of the standard optical fiber, the middle section of the optical fiber with the coating layer removed is heated close to the heating source, and the two ends of the optical fiber are fixed on an electrically controlled moving platform. As the heating softens the optical fiber, the platform stretches the optical

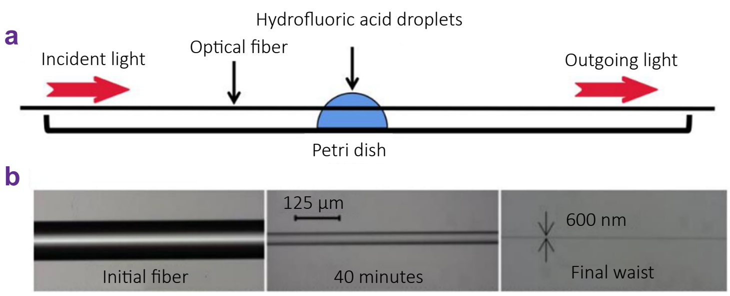

Fig. 11 | Hydrofluoric acid etching of a single-mode optical fiber. (a) Schematic diagram of the etching device. (b) Optical microscope pictures of the fiber being etched at different time points.

fiber at both ends with a certain force in order to obtain the specific required optical fiber dimensions[117], as shown in Fig. 12. According to the different heating methods, the fusion taper method can be divided into: electric heating fusion taper method[118], oxyhydrogen flame heating fusion taper method[119], laser heating fusion taper method[120] and high-temperature ceramic probe heating[121] and other methods. The melt-drawing cone method is currently the most mature and most promising technology for the industrialisation of micro-nano optical fiber manufacturing. The micro-nano optical fiber prepared by the melt-drawing cone method has a smooth surface, atomic level flatness, low optical transmission loss and better flexibility, and therefore is superior to other optical and mechanical properties. However, the above methods still have the problems of unstable heating temperature, environmental interference, or inability to further stretch the optical fiber, so related researchers proposed the two-step stretching method[122] and the self-modulation method, the two-step stretching method is developed on the basis of the fusion pulling cone method, and the operation process is to firstly wind the optical fiber preform that has already been stretched thinly on the tip of the rod sapphire, and then make the optical fiber softened and stretched again with the help of heat conduction by heating the sapphire rod. The fiber is softened and stretched again by heat conduction. Due to the uniform temperature distribution at the tip of the sapphire rod, it is possible to effectively stretch the fiber diameter to hundreds or even tens of nanometres. The self-modulated tensile cone method is designed by designing a special tensile cone platform, so that the optical fiber maintains a certain bending state during stretching, thus using the change of bending tension to uniformly apply the force. Specifically, at the beginning of stretching, the optical fiber is thicker, requiring a larger tension, bending stress is concentrated in the thick part; as the diameter of the optical fiber decreases, the required tension is gradually reduced, and the bending stress is concentrated in the finer part. The automatic migration of bending stresses helps to keep the forces on the fiber balanced, thus enabling it to be drawn finer. With the continuous improvement of the fused taper method, it has been possible to control the preparation of micro-nano optical fibers to meet the needs of various types of optical devices, and can achieve high repeatability and stability. It is foreseeable that the development of optical devices will usher in a new breakthrough with the maturity of the fused taper method.

4.3 Fabrication of photonic crystal fibers (PCFs)

The fabrication of photonic crystal fibers mainly relies on the stack-and-draw method, where silica capillaries are stacked in a designed pattern to form the preform, which is then drawn into a fiber under high temperature. This technique allows for precise control of the air-hole lattice and has been widely used for hollow-core and suspended-core PCFs. In recent years, alternative methods such as extrusion and 3D printing of preforms have been reported, enabling more flexible geometries and potentially large-scale production. The main challenges lie in maintaining uniformity of air holes during fiber drawing and ensuring reproducibility across long fiber lengths.

4.4 Fabrication of fiber gratings

Fiber gratings are most commonly inscribed by ultraviolet (UV) laser exposure using a phase mask, which remains the standard technique for fabricating FBGs with high precision and reproducibility. For advanced gratings such as tilted FBGs or localized gratings, femtosecond laser inscription offers high flexibility and three-dimensional localization of the refractive index change inside the fiber. Arc-discharge and mechanical pressure methods have also been explored for LPFG fabrication. These diverse inscription techniques enable tailored grating structures for different sensing

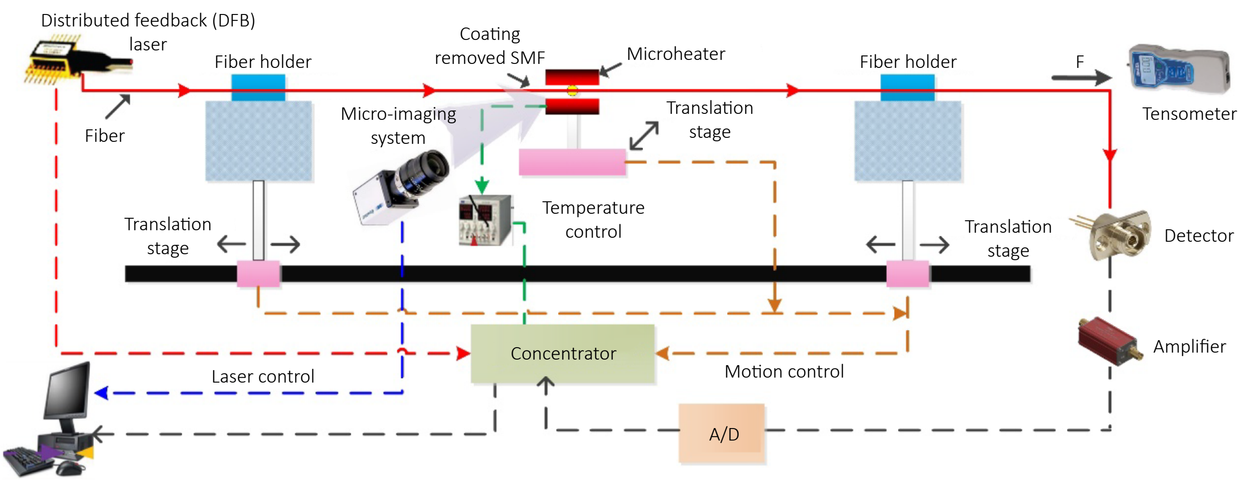

Fig. 12 | Schematic diagram of hot melt fiber pulling cone.

applications, but trade-offs exist between cost, inscription speed, and long-term stability.

5 Conclusions

In this paper, the theoretical basis and preparation method of fiber-optic microstructured sensors based on the swiftly passing wave principle are systematically discussed. Firstly, the generation mechanism of swiftly passing wave and its role in microstructured fiber optic sensing are introduced, and the high sensitivity and weak signal detection ability of swiftly passing wave make it show significant advantages in the fields of biosensing, environmental monitoring and industrial detection. Subsequently, the mainstream micro-nano optical fiber preparation methods, including chemical etching and high-temperature melt-drawing cone method, are summarized, among which the melt-drawing cone method is the most promising industrialized preparation technology due to its smooth surface, low loss and high repeatability. Comprehensive theoretical support is provided for the design of fiber-optic sensors based on swift wave, and a solid foundation is laid for the study of optimizing sensor performance.

6 Outlook and future perspectives

Looking forward, the development of evanescent-field-based fiber microstructure sensors is expected to evolve from the pursuit of single-parameter ultra-high sensitivity toward multi-objective optimization, where sensing performance, robustness, reproducibility, and manufacturability are considered simultaneously. From a structural perspective, different fiber architectures exhibit distinct development trajectories, challenges, and opportunities.

6.1 Micro-/nano-fiber-based sensors

Optical micro- and nanofibers will continue to play an important role in applications requiring ultra-high sensitivity and fast dynamic response, owing to their large evanescent-field fraction and strong light–matter interaction. Future development is expected to focus on robust packaging strategies, anti-fouling and anti-drift surface functionalization, and hybrid integration with gratings, resonators, or microfluidic components to enable multi-parameter sensing. However, challenges remain in terms of mechanical fragility, long-term stability, and batch-to-batch reproducibility. Addressing these issues will be essential for translating micro-/nano-fiber sensors from laboratory demonstrations to practical and deployable systems.

6.2 Photonic crystal fiber (PCF)-based sensors

For photonic crystal fiber sensors, future research is likely to emphasize application-oriented structural design, particularly for gas and chemical sensing. The intrinsic microchannel structures of PCFs provide unique advantages for gas infiltration, extended interaction length, and enhanced field overlap. Nevertheless, widespread deployment is still limited by challenges such as uniform inner-hole coating, repeatable filling processes, and reliable sealing and interconnection. Future efforts are expected to focus on simplified hole geometries, functional-material-assisted infiltration (e.g., MOFs or polymers), and standardized fabrication and packaging protocols to improve reproducibility and scalability.

6.3 Fiber grating-based sensors

Fiber grating sensors, including FBGs, LPFGs, TFBGs, excessively tilted gratings, and localized gratings, are expected to remain a cornerstone for physical, chemical, and biochemical sensing. Future trends include enhanced cladding-mode engineering through tilted or localized grating designs, multi-parameter decoupling strategies using cascaded or polarization-resolved gratings, and integration with plasmonic or functional coatings for improved biochemical sensitivity. Meanwhile, challenges such as polarization dependence, spectral complexity, and cross-sensitivity will need to be addressed through optimized structural design and advanced signal demodulation techniques.

6.4 Hybrid and intelligent fiber-optic sensing systems

An emerging trend in this field is the development of hybrid sensing systems that combine multiple structures and mechanisms, such as fiber gratings integrated with SPR/LSPR interfaces, micro-/nano-fibers, and optofluidic platforms. In parallel, data-driven and intelligent interrogation methods, including machine-learning-assisted demodulation and drift compensation, are expected to play an increasingly important role in improving sensing accuracy and long-term stability. Such hybrid and intelligent systems offer promising pathways toward practical, high-performance, and multifunctional fiber-optic sensors.

6.5 Toward practical deployment and standardization

Beyond structural and functional innovation, future progress will increasingly depend on addressing engineering and standardization challenges, including long-term stability, calibration strategies, packaging reliability, and performance benchmarking. Establishing commonly accepted evaluation metrics—such as detection limit, response time, cross-sensitivity coefficients, long-term drift, and repeatability—will be crucial for enabling fair comparison across different sensing platforms and accelerating real-world applications.

References

1. Li GR, Wong TW, Shih B et al. Bioinspired soft robots for deep-sea exploration. *Nat Commun* **14**, 7097 (2023).
2. Irfan MS, Ali MA, Khan T et al. MXene and graphene coated multi-functional fiber reinforced aerospace composites with sensing and EMI shielding abilities. *Compos Part A Appl Sci Manuf* **165**, 107351 (2023).
3. Liu WX, Cao HZ, Wen CF et al. Integrated photonic engine chips for interferometric fiber optic gyroscopes (invited). *Laser Optoelectron Prog* **61**, 1913012 (2024).
4. Nie ZY, Kwak JW, Han MD et al. Mechanically active materials and devices for bio‐interfaced pressure sensors—a review. *Adv Mater* **36**, 2205609 (2024).
5. Xue ZK, Guo Q, Liu SR et al. Fiber Bragg grating temperature and pressure sensor for oil and gas well. *Chin Opt* **14**, 1224–1230 (2021).
6. Babu A, Aazem I, Walden R et al. Electrospun nanofiber based TENGs for wearable electronics and self-powered sensing. *Chem Eng J* **452**, 139060 (2023).
7. Imas JJ, Matías IR, Del Villar I et al. All-fiber ellipsometer for nanoscale dielectric coatings. *Opto-Electron Adv* **6**, 230048 (2023).
8. Pan J, Wang Q, Gao SK et al. Knot-inspired optical sensors for slip detection and friction measurement in dexterous robotic manipulation. *Opto-Electron Adv* **6**, 230076 (2023).
9. Yang XZ, Yi YT, Lu WQ et al. D-shaped photonic crystal fiber based on surface plasmon resonance for low refractive index applications. *Opt Mater* **153**, 115612 (2024).
10. Ambrogi EK, Mirica KA. Electronic chemical sensors based on conductive framework materials. *Anal Chem* **97**, 4253–4274 (2025).
11. Liu SH, Yang H, Tang CJ et al. Highly sensitive photonic crystal optic fiber with annular stomatal arrangement for cervical cancer cell detection. *Phys Lett A* **548**, 130574 (2025).
12. Elsherif M, Salih AE, Muñoz MG et al. Optical fiber sensors: working principle, applications, and limitations. *Adv Photonics Res* **3**, 2100371 (2022).
13. Liu HH, Hu DJJ, Sun QZ et al. Specialty optical fibers for advanced sensing applications. *Opto-Electron Sci* **2**, 220025 (2023).
14. Jiao LZ, Zhong NB, Zhao XD et al. Recent advances in fiber-optic evanescent wave sensors for monitoring organic and inorganic pollutants in water. *TrAC Trends Anal Chem* **127**, 115892 (2020).
15. Bosch ME, Sánchez AJR, Rojas FS et al. Recent development in optical fiber biosensors. *Sensors* **7**, 797–859 (2007).
16. Zhang F, Li B, Zhang X et al. A highly sensitive fiber-tip temperature sensor based on enhanced Fresnel reflection induced by modified materials. *Ceram Int* **50**, 16463–16473 (2024).
17. Liu SC, Zhu PY, Xie FM et al. Gecko-inspired self-adhesive packaging for strain-free temperature sensing based on optical fibre Bragg gratings. *Sci Rep* **13**, 4148 (2023).
18. Cao RT, Ding HJ, Kim KJ et al. Metal-organic framework functionalized polymer coating for fiber optical methane sensors. *Sens Actuators B Chem* **324**, 128627 (2020).
19. Ding LY, Ruan YL, Li T et al. Nitric oxide optical fiber sensor based on exposed core fibers and CdTe/CdS quantum dots. *Sens Actuators B Chem* **273**, 9–17 (2018).
20. Zhou X, Deng QY, Yu WT et al. The rise of graphene photonic crystal fibers. *Adv Funct Mater* **32**, 2202282 (2022).
21. Li Z, Xiao YG, Liu F et al. *Operando* optical fiber monitoring of nanoscale and fast temperature changes during photo-electrocatalytic reactions. *Light Sci Appl* **11**, 220 (2022).
22. Niu PP, Jiang JF, Liu K et al. Fiber-integrated WGM optofluidic chip enhanced by microwave photonic analyzer for cardiac biomarker detection with ultra-high resolution. *Biosens Bioelectron* **208**, 114238 (2022).
23. Zhang YN, Gao J, Xia F et al. Microfiber knot resonators: structure, spectral properties, and sensing applications. *Laser Photonics Rev* **18**, 2300765 (2024).
24. Zhou ZR, Qiu ZJ, Li K et al. Review on demodulation methods for optic fiber Fabry-Perot sensors. *Opto-Electron Eng* **49**, 210411 (2022).
25. Zhao Y, Zhao H, Lv RQ et al. Review of optical fiber Mach-Zehnder interferometers with micro-cavity fabricated by femtosecond laser and sensing applications. *Opt Lasers Eng* **117**, 7–20 (2019).
26. Liu CY, Chen HL, Chen Q et al. Sagnac interferometer-based optical fiber strain sensor with exceeding free spectral measurement range and high sensitivity. *Opt Laser Technol* **159**, 108935 (2023).
27. Pang YN, Liu B, Liu J et al. Singlemode-multimode-singlemode optical fiber sensor for accurate blood pressure monitoring. *J Lightwave Technol* **40**, 4443–4450 (2022).
28. Li H, Li HB, Meng FY et al. All-fiber MZI sensor based on seven-core fiber and fiber ball symmetrical structure. *Opt Lasers Eng* **112**, 1–6 (2019).
29. Yan WC, Han Q, Chen YF et al. Fiber-loop ring-down interrogated refractive index sensor based on an SNS fiber structure. *Sens Actuators B Chem* **255**, 2018–2022 (2018).
30. Zhao Y, Tong RJ, Chen MQ et al. Relative humidity sensor based on hollow core fiber filled with GQDs-PVA. *Sens Actuators B Chem* **284**, 96–102 (2019).
31. Yin SY, Guo Q, Liu SR et al. Three-dimensional multichannel waveguide grating filters. *Opto-Electron Sci* **3**, 240003 (2024).
32. Liao CR, Xiong C, Zhao JL et al. Design and realization of 3D printed fiber-tip microcantilever probes applied to hydrogen sensing. *Light Adv Manuf* **3**, 3–13 (2022).
33. Zhang L, Shang XG, Cao SM et al. Optical steelyard: high-resolution and wide-range refractive index sensing by synergizing Fabry-Perot interferometer with metafibers. *PhotoniX* **5**, 24 (2024).
34. Yi YX, Yi Z, Zhou ZG et al. Structural design and analysis of D-type elliptical open-loop photonic crystal fiber temperature sensor based on SPR. *Phys B Condens Matter* **715**, 417549 (2025).
35. Yang XZ, Song QJ, Ma C et al. A methane concentration sensor with heightened sensitivity and D-shaped cross-section U-shaped channel utilizing the principles of surface plasmon resonance. *Phys E Low-Dimens Syst Nanostruct* **161**, 115954 (2024).
36. Du HL, Li B, Zhu AS et al. Research on refractive index and temperature measurement based on S-shaped SPR fiber sensor. *J Lightwave Technol* **43**, 3331–3337 (2025).
37. Ning W, Hu SM, Zhou C et al. An ultrasensitive J-shaped optical fiber LSPR aptasensor for the detection of *Helicobacter pylori*. *Anal Chim Acta* **1278**, 341733 (2023).
38. Luo ZW, Cheng Y, He L et al. T-shaped aptamer-based LSPR biosensor using Ω-shaped fiber optic for rapid detection of SARS-CoV-2. *Anal Chem* **95**, 1599–1607 (2023).
39. Zhang L, Zhen YQ, Tong LM. Optical micro/nanofiber enabled tactile sensors and soft actuators: a review. *Opto-Electron Sci* **3**, 240005 (2024).
40. Sun N, Gan Y, Wu YJ et al. Single-beam optical trap-based surface-enhanced Raman scattering optofluidic molecular fingerprint spectroscopy detection system. *Opto-Electron Adv* **8**, 240182 (2025).
41. Jiang XF, Qavi AJ, Huang SH et al. Whispering-gallery sensors. *Matter* **3**, 371–392 (2020).
42. Jing JY, Liu K, Jiang JF et al. Performance improvement approaches for optical fiber SPR sensors and their sensing applications. *Photon Res* **10**, 126–147 (2022).
43. Gomes AD, Bartelt H, Frazão O. Optical vernier effect: recent advances and developments. *Laser Photonics Rev* **15**, 2000588 (2021).

44. Sharma AK, Gupta J, Sharma I. Fiber optic evanescent wave absorption-based sensors: a detailed review of advancements in the last decade (2007–18). *Optik* **183**, 1008–1025 (2019).
45. Khonina SN, Kazanskiy NL, Butt MA. Optical fibre-based sensors—an assessment of current innovations. *Biosensors* **13**, 835 (2023).
46. Portosi V, Laneve D, Falconi MC et al. Advances on photonic crystal fiber sensors and applications. *Sensors* **19**, 1892 (2019).
47. Gao H, Hu HF, Zhan QW. Tailoring temperature response for a multimode fiber. *Opto-Electron Sci* **4**, 240004 (2025).
48. Liu Y, Strum R, Stiles D et al. Digital phase demodulation for low-coherence interferometry-based fiber-optic sensors. *Opt Commun* **411**, 27–32 (2018).
49. Gupta BD, Verma RK. Surface plasmon resonance - based fiber optic sensors: principle, probe designs, and some applications. *J Sens* **2009**, 979761 (2009).
50. Lee S, Song H, Ahn H et al. Fiber-optic localized surface plasmon resonance sensors based on nanomaterials. *Sensors* **21**, 819 (2021).
51. Wang Q, Zhang DY, Qian YZ et al. Research on fiber optic surface plasmon resonance biosensors: a review. *Photonic Sens* **14**, 240201 (2024).
52. Salman NA. Preparation of tapered photonic crystal fiber material to employ the evanescent wave for sensing applications. *Mater Today Proc* **61**, 681–685 (2022).
53. Dai TT, Yi YT, Yi Z et al. Photonic crystal fiber based on surface plasmon resonance used for two parameter sensing for magnetic field and temperature. *Photonics* **11**, 784 (2024).
54. Guo T, Liu F, Guan BO et al. Tilted fiber grating mechanical and biochemical sensors. *Opt Laser Technol* **78**, 19–33 (2016).
55. Feng DY, Zhou WJ, Qiao XG et al. Compact optical fiber 3D shape sensor based on a pair of orthogonal tilted fiber Bragg gratings. *Sci Rep* **5**, 17415 (2015).
56. Guo X, Ying YB, Tong LM. Photonic nanowires: from subwavelength waveguides to optical sensors. *Acc Chem Res* **47**, 656–666 (2014).
57. Zhang JB, Fang HB, Wang P et al. Optical microfiber or nanofiber: a miniature fiber-optic platform for nanophotonics. *Photonics Insights* **3**, R02 (2024).
58. Zhu HT, Luo JX, Dai Q et al. Spatiotemporal hemodynamic monitoring via configurable skin-like microfiber Bragg grating group. *Opto-Electron Adv* **6**, 230018 (2023).
59. Zhang L, Lou JY, Tong LM. Micro/nanofiber optical sensors. *Photonic Sens* **1**, 31–42 (2011).
60. Zhang L, Tang Y, Tong LM. Micro-/nanofiber optics: merging photonics and material science on nanoscale for advanced sensing technology. *iScience* **23**, 100810 (2020).
61. Li W, Chen BG, Meng C et al. Ultrafast all-optical graphene modulator. *Nano Lett* **14**, 955–959 (2014).
62. Gorajoobi SB, Murugan GS, Zervas MN. Design of rare-earth-doped microbottle lasers. *Opt Express* **26**, 26339–26354 (2018).
63. Tang Y, Liu HT, Pan J et al. Optical micro/nanofiber-enabled compact tactile sensor for hardness discrimination. *ACS Appl Mater Interfaces* **13**, 4560–4566 (2021).
64. Yu W, Yao N, Pan J et al. Highly sensitive and fast response strain sensor based on evanescently coupled micro/nanofibers. *Opto-Electron Adv* **5**, 210101 (2022).
65. Ma SQ, Wang XY, Li P et al. Optical micro/nano fibers enabled smart textiles for human-machine interface. *Adv Fiber Mater* **4**, 1108–1117 (2022).
66. Yao JQ, Wang R, Miao YP et al. Novel photonic functional devices based on liquid-filling microstructured optical fibers. *Chin J Lasers* **40**, 101002 (2013).
67. Jing JY, Liu K, Jiang JF et al. Highly sensitive and stable probe refractometer based on configurable plasmonic resonance with nano-modified fiber core. *Opto-Electron Adv* **6**, 220072 (2023).
68. Xiao LM, Jin W, Demokan MS. Photonic crystal fibers confining light by both index-guiding and bandgap-guiding: hybrid PCFs. *Opt Express* **15**, 15637–15647 (2007).
69. Chen K, Zhou X, Cheng X et al. Graphene photonic crystal fibre with strong and tunable light-matter interaction. *Nat Photonics* **13**, 754–759 (2019).
70. Yang JC, Shen R, Yan PX et al. Fluorescence sensor for volatile trace explosives based on a hollow core photonic crystal fiber. *Sens Actuators B Chem* **306**, 127585 (2020).
71. Tong RJ, Wang Y, Zhao KJ et al. Surface plasmon resonance optical fiber sensor for relative humidity detection without temperature crosstalk. *Opt Laser Technol* **150**, 107951 (2022).
72. Wang HR, Wu MY, Zheng SC et al. Surface plasmon resonance sensor based on seven-core photonic crystal fiber for refractive index and temperature measurement. *Opt Laser Technol* **164**, 109511 (2023).
73. Yao SY, Yu Y, Qin SP et al. Research on optimization of magnetic field sensing characteristics of PCF sensor based on SPR. *Opt Express* **30**, 16405–16418 (2022).
74. Ehyaee A, Rahmati A, Bosaghzadeh A et al. Machine learning-enhanced surface plasmon resonance based photonic crystal fiber sensor. *Opt Express* **32**, 13369–13383 (2024).
75. Guo T. Review on plasmonic optical fiber grating biosensors. *Acta Opt Sin* **38**, 328006 (2018).
76. Xue XB, Han XL, Li WJ et al. *Operando* battery monitoring: lab-on-fiber electrochemical sensing technologies. *Laser Photonics Rev* **18**, 2301298 (2024).
77. Sahota JK, Gupta N, Dhawan D. Fiber Bragg grating sensors for monitoring of physical parameters: a comprehensive review. *Opt Eng* **59**, 060901 (2020).
78. Dong XY, Zhang H, Liu B et al. Tilted fiber Bragg gratings: principle and sensing applications. *Photonic Sens* **1**, 6–30 (2011).
79. Rego G. A review of refractometric sensors based on long period fibre gratings. *Sci World J* **2013**, 913418 (2013).
80. Loyez M, Hassan EM, Lobry M et al. Rapid detection of circulating breast cancer cells using a multiresonant optical fiber aptasensor with plasmonic amplification. *ACS Sens* **5**, 454–463 (2020).
81. Liu C, Cai Q, Xu BJ et al. Graphene oxide functionalized long period grating for ultrasensitive label-free immunosensing. *Biosens Bioelectron* **94**, 200–206 (2017).
82. Huang Y, Lin WF, Zhang ZR et al. Photothermal-assisted for ultrafast response acetone sensing with ZIF-90/GO coated microfiber long period gratings. *Chem Eng J* **473**, 145479 (2023).
83. Wang YN, Liao ZJ, Li J et al. ZnOHF-ZnO nanomaterial-coated macro-bend fiber triethylamine gas sensor working at room temperature. *Sens Actuators B Chem* **411**, 135733 (2024).
84. Zhou WC, Wei YL, Wang Y et al. Ultrasensitive interferometers based on zigzag-shaped tapered optical microfibers operating at the dispersion turning point. *Opt Express* **29**, 36926–36935 (2021).
85. Hu SQ, Chen JY, Liang JH et al. Hyperbolic-metamaterials-based SPR temperature sensor enhanced by a nanodiamond-PDMS hybrid for high sensitivity and fast response. *ACS Appl Mater Interfaces* **14**, 42412–42419 (2022).
86. Chen YF, Lin QY, Cheng HD et al. Nanodiamond-based optical-fiber quantum probe for magnetic field and biological sensing. *ACS Sens* **7**, 3660–3670 (2022).
87. Menon S, Usha SP, Manoharan H et al. Metal-organic framework-based fiber optic sensor for chromium (VI) detection. *ACS Sens* **8**, 684–693 (2023).
88. Jean-Ruel H, Albert J. Recent advances and current trends in optical fiber biosensors based on tilted fiber Bragg gratings. *TrAC Trends Anal Chem* **174**, 117663 (2024).

89. Lv JW, Wang JX, Yang L et al. Recent advances of optical fiber biosensors based on surface plasmon resonance: sensing principles, structures, and prospects. *Sens Diagn* **3**, 1369–1391 (2024).
90. Mustapha Kamil Y, Abu Bakar MH, Zainuddin NH et al. Progress and trends of optical microfiber-based biosensors. *Biosensors* **13**, 270 (2023).
91. Butt MA, Voronkov GS, Grakhova EP et al. Environmental monitoring: a comprehensive review on optical waveguide and fiber-based sensors. *Biosensors* **12**, 1038 (2022).
92. Ramola A, Shakya AK, Kumar V et al. Recent advances in photonic crystal fiber-based SPR biosensors: design strategies, plasmonic materials, and applications. *Micromachines* **16**, 747 (2025).
93. Lu MD, Wang C, Fan RZ et al. Review of fiber-optic localized surface plasmon resonance sensors: geometries, fabrication technologies, and bio-applications. *Photonic Sens* **14**, 240202 (2024).
94. Gao S, Yang XY, Wang SJ et al. Review of optical fiber optofluidic chemical sensors and biosensors. *Photonic Sens* **15**, 250134 (2025).
95. Xi JW, Sun H, Li JZ et al. Tilted fiber Bragg grating sensor based on surface plasmon resonance and electrospinning for glucose detection. *Microchem J* **204**, 110978 (2024).
96. Yao N, Wang XY, Ma SQ et al. Single optical microfiber enabled tactile sensor for simultaneous temperature and pressure measurement. *Photonics Res* **10**, 2040–2046 (2022).
97. Ren HR, Jang J, Li CH et al. An achromatic metafiber for focusing and imaging across the entire telecommunication range. *Nat Commun* **13**, 4183 (2022).
98. Rahmani B, Loterie D, Konstantinou G et al. Multimode optical fiber transmission with a deep learning network. *Light Sci Appl* **7**, 69 (2018).
99. Li J, Zhang MJ. Physics and applications of Raman distributed optical fiber sensing. *Light Sci Appl* **11**, 128 (2022).
100. Jiang SL, Chen FF, Zhao Y et al. Broadband all-fiber optical phase modulator based on photo-thermal effect in a gas-filled hollow-core fiber. *Opto-Electron Adv* **6**, 220085 (2023).
101. Zhong NB, Liao Q, Zhu X et al. A fiber-optic sensor for accurately monitoring biofilm growth in a hydrogen production photobioreactor. *Anal Chem* **86**, 3994–4001 (2014).
102. Gloge D. Weakly guiding fibers. *Appl Opt* **10**, 2252–2258 (1971).
103. Olshansky R. Mode coupling effects in graded-index optical fibers. *Appl Opt* **14**, 935–945 (1975).
104. Chen ZY, Liu MS, Cheng SB et al. Bilayer graphene metasurface with dynamically reconfigurable terahertz perfect absorption. *Curr Appl Phys* **80**, 282–290 (2025).
105. Ai Z, Yi YT, Yang H et al. TiN-Ti ultra-broadband solar absorber: efficient heat absorption and high thermal stability. *Phys Lett A* **556**, 130827 (2025).
106. Kuznetsov AG, Kharenko DS, Babin SA et al. Ultralong fibre-optic distributed Raman temperature sensor. *Quantum Electron* **47**, 967–970 (2017).
107. Tanner MG, Dyer SD, Baek B et al. High-resolution single-mode fiber-optic distributed Raman sensor for absolute temperature measurement using superconducting nanowire single-photon detectors. *Appl Phys Lett* **99**, 201110 (2011).
108. Satija J, Punjabi NS, Sai VVR et al. Optimal design for U-bent fiber-optic LSPR sensor probes. *Plasmonics* **9**, 251–260 (2014).
109. Shao LX, Yang H, Yi Z et al. Graphene terahertz metamaterials absorber with multiple absorption peaks and adjustable incident polarization angle. *Phys B Condens Matter* **714**, 417427 (2025).
110. Wu GX, Zhu RZ, Lu YQ et al. Optical scanning endoscope via a single multimode optical fiber. *Opto-Electron Sci* **3**, 230041 (2024).
111. Liu JX, Li HP, Noh HY et al. Urban sensing using existing fiber-optic networks. *Nat Commun* **16**, 3091 (2025).
112. Lalam N, Westbrook P, Naeem K et al. Pilot-scale testing of natural gas pipeline monitoring based on phase-OTDR and enhanced scatter optical fiber cable. *Sci Rep* **13**, 14037 (2023).
113. Li Z, Chen JX, Li LZ et al. Exceptional-point-enhanced sensing in an all-fiber bending sensor. *Opto-Electron Adv* **6**, 230019 (2023).
114. Gaston A, Lozano I, Perez F et al. Evanescent wave optical-fiber sensing (temperature, relative humidity, and pH sensors). *IEEE Sens J* **3**, 806–811 (2003).
115. Lu P, Lalam N, Badar M et al. Distributed optical fiber sensing: review and perspective. *Appl Phys Rev* **6**, 041302 (2019).
116. Zhang EJ, Sacher WD, Poon JKS. Hydrofluoric acid flow etching of low-loss subwavelength-diameter biconical fiber tapers. *Opt Express* **18**, 22593–22598 (2010).
117. Kang Y, Liu KY, Xie Y et al. Fabrication methods and high-precision diameter control techniques of optical micro-/nanofibers. *Sci Sin Phys Mech Astronomica* **50**, 084212 (2020).
118. Saxena MK, Raju SDVSJ, Arya R et al. Optical fiber distributed temperature sensor using short term Fourier transform based simplified signal processing of Raman signals. *Measurement* **47**, 345–355 (2014).
119. Hu J, Lin WH, Shao LY et al. High-resolution tumor marker detection based on microwave photonics demodulated dual wavelength fiber laser sensor. *Opto-Electron Adv* **7**, 240105 (2024).
120. Jiang WW, Zhao RF, Wei Y et al. Spectral characteristics of Bragg fiber grating based on fused taper fiber. *Chin J Lasers* **37**, 2565–2569 (2010).
121. Zhou GR, You H, Zhu WL et al. Application of optical micro-fibres decorated with a co-doped Er^{3+}/Yb^{3+} silica film with fast desorption response for environmental cleanliness measurement of a laser facility. *Measurement* **246**, 116731 (2025).
122. Tong LM, Gattass RR, Ashcom JB et al. Subwavelength-diameter silica wires for low-loss optical wave guiding. *Nature* **426**, 816–819 (2003).

Acknowledgements

The authors are grateful to the support by National Natural Science Foundation of China (Nos. 51606158, 12104402).

Competing interests

The authors declare no competing financial interests.

Published by Editorial Office of *Opto-Electronic Science*, Institute of Optics and Electronics, Chinese Academy of Sciences.

Opto-Electronic Journals Group
www.oejournal.org

Scan for Article PDF